Properties and Structure of Aromatic Ester Solvents

Santiago Aparicio,* Rafael Alcalde, María J. Dávila, Begoña García, and José M. Leal

Departamento de Química, Universidad de Burgos, 09001 Burgos, Spain

Received: December 13, 2006; In Final Form: February 1, 2007

This paper reports on an experimental and theoretical study of the aromatic ester solvents family. Several compounds were selected to analyze the different factors that influence their liquid-state properties and structures. The pressure−volume−temperature behavior of these fluids was measured accurately over wide temperature and pressure ranges and correlated successfully with the empirical TRIDEN equation. From the measured data the relevant derived coefficients of isothermal compressibility, isobaric expansibility, and internal pressure were calculated. The statistical associating fluid theory (SAFT) and perturbed chain statistical associating fluid theory (PC-SAFT) molecularly based equations of state were used to predict the PVT behavior with model parameters obtained from the correlation of available saturation literature data; the results provided by PC-SAFT equations of state were clearly superior for all of the studied solvents. The fluid's molecular level structure was studied by quantum computations at the B3LYP/6-311++g** level and classical molecular dynamics simulations in the NPT ensemble with the OPLS-AA forcefield. Molecular parameters, such as torsional barriers or cluster energetics, were analyzed as a function of ester structures. The molecular dynamics study provides, on one hand, theoretical values of thermophysical properties, which are compared with the experimental ones, and, on the other hand, valuable molecular level structural information. On the basis of both macroscopic and microscopic studies complex fluid structures were inferred with important effects arising from the geometries of the studied molecules and from the existence of remarkable intermolecular forces of dominating dipolar nature.

Introduction

The knowledge of properties and structures of solvents is extremely important from both industrial and theoretical viewpoints.[1,2] Solvents play a central role in many processes, and thus the use of the most adequate compound may improve the quality of the final product, the economics of the process, and the environmental aspects of the whole production cycle.[3−5] Thus, a proper process design needs to take into account the selection of the best solvent;[5] this requires a priori knowledge of fluid properties in the wide pressure and temperature ranges for which many industrial operations have to be designed.[6,7] These properties are known only at low pressures and in narrow temperature ranges for most of the fluids, which is clearly insufficient, and thus the industrial use of new solvent families may be frequently hindered by the absence of accurate studies on their thermophysical behavior. The most reliable way to obtain these properties is through systematic experimental studies, but the accurate measurement of thermophysical properties requires considerable experimental skill and complex equipment; mainly if wide pressure ranges are considered with the derived financial and time constraints,[8] then theoretical models that can correlate and predict properties with the demanded accuracy are also required. Anyhow, these models should be tested against reliable experimental data, and then both approaches may be considered as complementary at this moment. However, the development of models requires the knowledge of fluid structure at the molecular level, including both intermolecular forces and facts derived from the molecular sizes and shapes; considering that the present state of the liquid-state theories does not allow us to infer accurately macroscopic property predictions for most of the complex fluids required,[9] the study of microscopic fluids structure through molecular modeling and its comparison with experimental macroscopic studies may provide a valuable tool to connect both approaches to debug the available thermophysical models and to develop new ones with deeper theoretical foundations.

Aromatic esters are a valuable family of molecules for a number of important technological applications. The presence of the polarizable aromatic π-electron system in the vicinity of the dipolar ester group, together with their hydrophobic and aprotic character, confer these molecules a highly selective solvent ability that is used for applications in fields such as cosmetic formulations, polymer science, dye carriers in fibers industry and several synthesis processes among others. In spite of their technological and theoretical importance, few systematic studies[10] on the properties and structure of aromatic esters, pure or mixed, have been reported and, as far as we know, any at pressures far from the ambient one. Thus, as a continuation of previous works,[11] six compounds belonging to this family were selected to analyze different structural features of fluid properties and structures: (i) methyl (MB), ethyl (EB), propyl (PB), and butylbenzoate (BB) to study the alkylic chain length effect; (ii) phenylacetate (PA) to analyze the effect of aromatic ring position related to the ester group by comparison with MB; and (iii) methylsalicylate (MS) to consider the structural changes arising from the presence of a hydrogen-bonding hydroxilic group in the ester aromatic ring. In this work the experimental pressure−volume−temperature (PVT) behavior of pure aromatic esters is reported in the 278.15−358.15 K and 0.1−60 MPa ranges; from these readings the isobaric thermal expansibility, isothermal compressibility,

* Author to whom correspondence should be addressed. E-mail: sapar@ubu.es.

10.1021/jp068560t CCC: $37.00
Published on Web 04/06/2007

and internal pressure were calculated. On one hand, the above properties are required for both thermodynamic calculations and operations such as phase separation, mass transfer, power requirements, or pumping; on the other hand, these data may also provide substantial information on the fluid structure and molecular level interactions.

The modeling of the PVT behavior of fluids is commonly described by the use of the so-called equations of state (EOS's), which are efficient and simple tools for the representation of the PVT properties over wide ranges of pressure and temperature.[12] Since the pioneering work by van der Waals, literally hundreds of EOS's have been put forward with variable degrees of success. Although cubic EOS's (derived from van der Waals' approach) have played a pivotal role both in modeling and in the development of fluid theories, and hence their popularity due mainly to the ease of handling provided by their simplicity, they suffer from several drawbacks, in particular an inaccurate representation of fluid properties in wide pressure and temperature ranges.[13] Therefore, cubic EOS's have given way to molecularly based EOS's, with a broader theoretical background capable of separating the interactions and quantifying the effects of fluid structure on bulk properties and phase behavior.[12] Among the different approaches available for the development of molecularly based EOS's, due to the lower computational costs and wide pressure and temperature ranges covered with high accuracy, those based on Wertheim's perturbation theory[14] have received growing recognition, in both academia and industry, giving rise to a set of EOS's known as statistical associating fluid theory (SAFT). The original SAFT approach developed by Huang and Radosz[15] and the perturbed chain (PC-SAFT)[16] version were applied in this work to predict the esters' PVT behavior. Model parameters were obtained from the correlation of literature available saturation data and used to predict the PVT behaviors that are compared with the experimental ones to check the reliability of each EOS.

Finally, molecular modeling is a powerful tool that provides a deeper insight into the structure of condensed phases; hence, to complete the information drawn from macroscopic measurements, a study of the six aromatic esters through quantum computations of isolated molecules and small clusters was carried out at the density functional theory (DFT) level. This work was completed with classical molecular dynamics simulations in the NPT ensemble that provide predictions of macroscopic properties, such as density or vaporization enthalpies, which are compared with experimental ones, together with valuable structural and dynamic information.

Thus, to recap, this work reports a study on the liquid-phase properties and structure of industrially relevant compounds from different viewpoints. The combined use of accurate thermophysical data in wide temperature and pressure ranges together with their modeling according to state-of-the-art EOS's and the molecular approach provided by the molecular modeling studies allow us to obtain a very detailed picture of the fluid structure and of the relation among microscopic features and macroscopic properties, which is of great importance not only for theoretical but also for practical industrial purposes.

Experimental Section

Solvents. MB (99.9%, GC purity), EB (99.9%), PB (98.7%), BB (99.1%), PA (99.5%), and MS (99.5%) were purchased from Aldrich and Fluka and stored out of light over Fluka Union Carbide 0.4 nm molecular sieves to avoid moisture absorption; prior to measurements they were degassed with ultrasound and used without further purification.

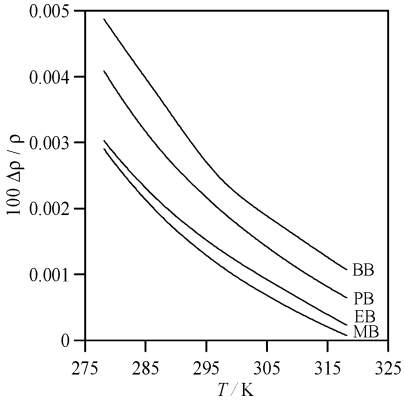

Figure 1. Percentage deviation between corrected and uncorrected density data at 0.1 MPa according to eq 1 with dynamic viscosity data from ref 11f.

Instruments and Procedures. The apparatus used in the PVT measurements was previously described in detail.[17] The system is installed around a high-pressure vibrating tube densimeter. The cell temperature was controlled by a Julabo F32 circulating bath; a calibrating Pt100 platinum sensor located in the measuring cell connected to a AΣΔF250 unit measures the temperature to $\pm 1 \times 10^{-2}$ K. The circuit pressure was controlled and measured by a Ruska 7615 digital pressure controller. The pressure was kept constant to $\pm 5 \times 10^{-3}$ MPa by the controller and measured to $\pm 1 \times 10^{-2}$ MPa with a pressure sensor. The pressurizing fluid was separated from the sample by a high-pressure liquid-to-liquid separator (Pressurements T3600E), which contained a Teflon diaphragm to send out the pressure. The pressure transducer and thermometer were previously calibrated through well-defined and traceable procedures. The whole system is computer-controlled by specially developed software that makes obtaining large amounts of accurate data feasible. For proper apparatus calibration a 14-parameter equation was used[17] with *n*-hexane (Fluka, 99.9%) and water (Millipore, resistivity 18.2 mΩ cm) as reference fluids.[18] It is well-known that density measurements through a vibrating tube apparatus are affected in a certain manner by the sample viscosity, and thus the uncertainty in measurements might increase if viscosity corrections are disregarded.[19] Corrections rely on both the existence of experimental viscosity data in the pressure and temperature ranges considered and properly defined and evaluated damping equations; thus, several expressions have been suggested.[19] In this work, the correction factor can be evaluated according to eq 1[19a,b]

$$\frac{\Delta\rho}{\rho} = (-0.5 + 0.45\sqrt{\eta})10^{-4} \qquad (1)$$

where ρ stands for the raw density data obtained according to the above procedure, $\Delta\rho$ is the difference between the raw and corrected density data, and η is the sample dynamic viscosity (mPa s). The viscosity effect on measurements was analyzed only at atmospheric pressure because of the absence of experimental high-pressure viscosity data; Figure 1 plots the viscosity effect on the measured densities, showing low deviations between corrected and uncorrected values; although viscosity effects at higher pressures will be more important, considering the low viscosity of the studied esters no corrections were included in the reported data because these would be below the accuracy limit; thus taking into account all factors involved in the density determination, an accuracy of $\pm 1 \times 10^{-4}$ g cm^{-3}

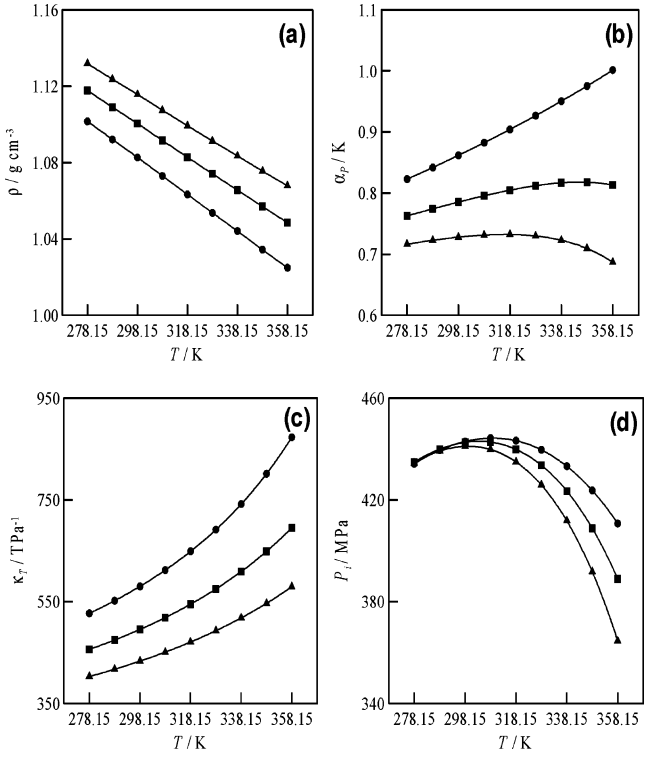

Figure 2. Temperature effect on the thermophysical properties of MB at different pressures: (a) density, ρ; (b) isobaric expansibility, α_P; (c) isothermal compressibility, κ_T; (d) internal pressure, P_i, (●) 0.1 MPa, (■) 30 MPa, and (▲) 60 MPa.

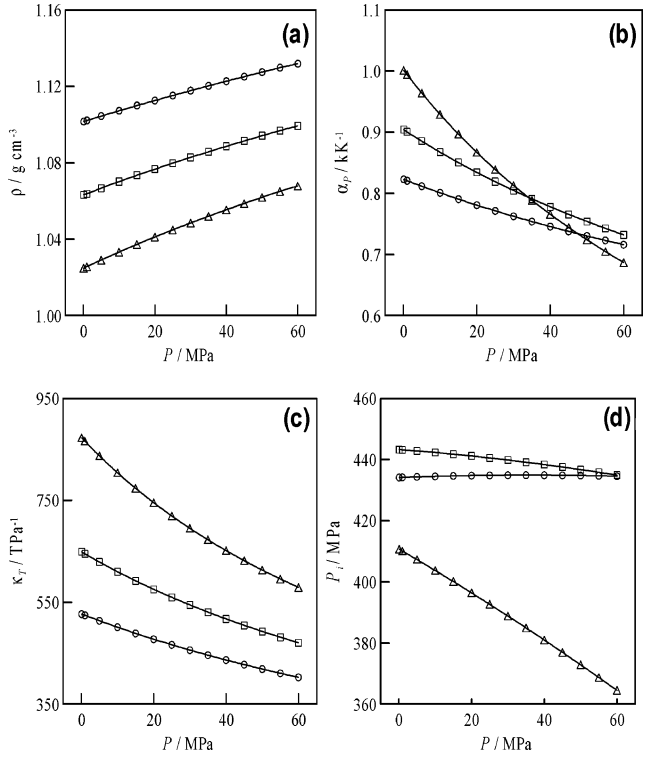

Figure 3. Pressure effect on the thermophysical properties of MB at different temperatures: (a) density, ρ; (b) isobaric expansibility, α_P; (c) isothermal compressibility, κ_T; (d) internal pressure, P_i, (○) 278.15 K , (□) 318.15 K, and (△) 358.15 K.

can be inferred for experimental raw density data without viscosity corrections.

Quantum Calculations. Quantum calculations were carried out with the Gaussian 03 package[20] according to DFT, using the Becke gradient-corrected exchange functional[21] and Lee−Yang−Parr correlation functional[22] with three parameters (B3LYP)[23] method. To describe properly electrons far from and close to the nuclei it is important to use large and flexible basis sets; here 6-311++g** was used. Atomic charges were calculated to fit the electrostatic potential[24] according to the Merz−Singh−Kollman (MK)[25]scheme; the fitting procedure was also constrained to reproduce the overall molecular dipole moment. Charges calculated using the MK scheme show a small dependence on the computational method and basis set employed, and thus they are considered clearly superior to Mulliken charges.

Molecular Dynamics Simulations. Classical molecular dynamics simulations were carried out using the TINKER molecular modeling package,[26a] which is a highly reliable and efficient tool that has been applied for systems of a very different nature.[26b−e] All simulations were performed in the NPT ensemble at 298.15 K and 0.1 MPa; the Nosé−Hoover method[27] was used to control the temperature and pressure of the simulation system. The motion equations were solved using the Verlet Leapfrog integration algorithm.[28] The molecular geometries were restrained according to the SHAKE algorithm.[29] Long-range electrostatic interactions were treated with the smooth particle mesh Ewald method.[30] Simulations were carried out for liquid and vapor phases, the last ones to calculate intermolecular energy. The simulated systems consist of cubic boxes with 250 molecules to which periodic boundary conditions were applied in three directions. The liquid box sizes were established according to the experimental densities whereas vapor ones were selected by expanding liquid ones to obtain a volume large enough (density of ~0.01 g cm^{-3}) to make all intermolecular interactions negligible. The simulations were performed using a cutoff radius of $L/2$ Å for the nonbonded interactions, L being the box side. Initial boxes were generated using the PACKMOL program[31a] that uses the BOX-QUACAN[31b] local-minimization method to obtain adequate starting configurations. These boxes were minimized according to the MINIMIZE program in the TINKER package to a 0.01 kcal mol^{-1} Å^{-1} root-mean-square (rms) gradient, then several heating and quenching steps in the NVT ensemble up to 500 K were performed after which a 100 ps NVT equilibration molecular dynamics simulation was run at 298 K; finally, from the output NVT simulation configuration, a run of 500 ps (time step of 1 fs) in the NPT ensemble at 298 K and 0.1 MPa was run, from which the first 100 ps were used to ensure equilibration (checked through constant energy) and the remaining 400 ps for data collection. Aromatic esters were described according to the so-called optimized potential for liquid simulations (all-atom version) OPLS-AA.[32] This model has been applied successfully to compute liquid-state properties for different systems.[33] MK charges obtained through B3LYP/6-311++g** calculations were used in the simulations.

Results and Discussion

PVT Behavior. Experimental and calculated thermophysical properties of aromatic esters in the 278.15−358.15 K and 0.1−60 MPa ranges are listed in Tables S1−S5 of the Supporting Information and plotted in Figures 2−5. The experimental compressed liquid densities were correlated with temperature and pressure according to the TRIDEN 10-parameter equation,[34] which combines the modified Rackett equation for saturation

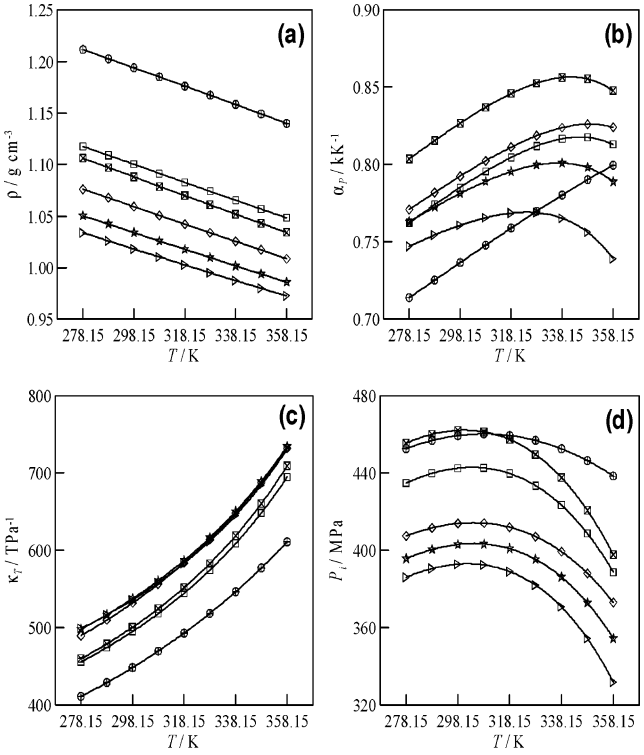

Figure 4. Temperature effect on the thermophysical properties of aromatic esters at 30 MPa: (a) density, ρ; (b) isobaric expansibility, α_P; (c) isothermal compressibility, κ_T; (d) internal pressure, P_i, (□) MB, (◇) EB, (☆) PB, (right-facing open triangle) BB, (open square with cross) PA, and (⊕) MS.

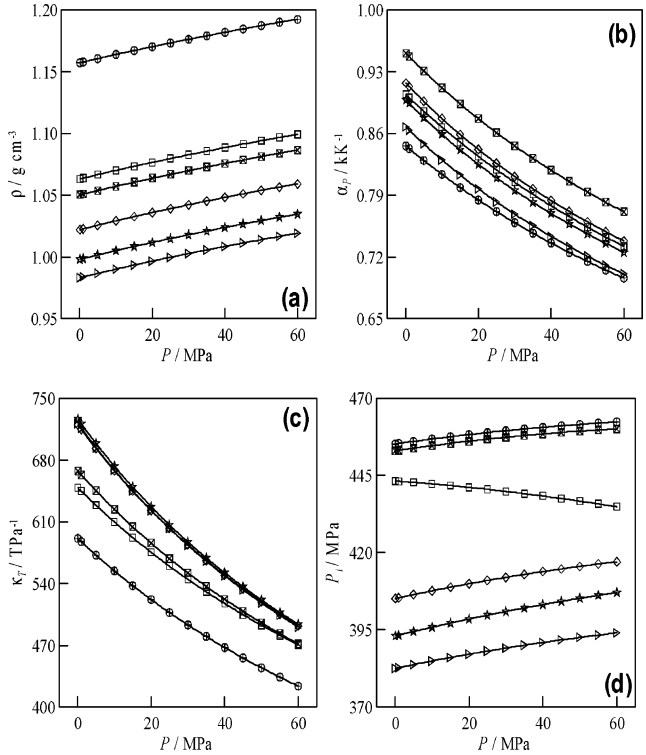

Figure 5. Pressure effect on the thermophysical properties of aromatic esters at 318.15 K: (a) density, ρ; (b) isobaric expansibility, α_P; (c) isothermal compressibility, κ_T; (d) internal pressure, P_i, (□) MB, (◇) EB, (☆) PB, (right-facing open triangle) BB, (open square with cross) PA, and (⊕) MS.

densities with Tait's equations for isothermal compressed densities, eqs 2−4

$$\rho_0 = \frac{A_R}{B_R^{[1+(1-T/C_R)D_R]}} \tag{2}$$

$$\rho = \frac{\rho_0}{1 - C_T \ln \dfrac{B_T + P}{B_T + P_0}} \tag{3}$$

$$B_T = b_0 + b_1 \frac{T}{E_T} + b_2\left(\frac{T}{E_T}\right)^2 + b_3\left(\frac{T}{E_T}\right)^3 \tag{4}$$

The reference pressure $P_0 = 0.1$ MPa was used at all temperatures, and the corresponding reference densities, ρ_0, were correlated with eq 2, the C_T Tait parameter being temperature-independent. The correlation parameters were deduced using a Levenberg−Marquardt least-squares algorithm, and the optimal fitting was assessed by the percentage of absolute average deviation (AAD)

$$\mathrm{AAD} = \frac{100}{N}\sum_{j=1}^{N}\left|\frac{\rho_{i,\mathrm{EXP}} - \rho_{i,\mathrm{CAL}}}{\rho_{i,\mathrm{EXP}}}\right|$$

where N is the number of data pairs. Table S2 summarizes the fitting parameters deduced. The flexibility of the empirical TRIDEN fitting equation, arising from the combination of different independent equations, together with the ability to obtain relaible extrapolations for both temperature and pressure are the main advantages of this approach.

Different plots of thermophysical properties are reported along Figures 2−5 to study the different effects on solvent properties: temperature effect along isobars, Figure 2, pressure effect along isotherms, Figure 3, temperature effect along isobars for different esters, Figure 4; pressure effect along isotherms for different esters, Figure 5. As usual, the density of each fluid decreases as temperature rises along isobars and increases as pressure rises along isotherms, Figures 2a−5a. For alkylbenzoates (MB−BB), the density decreases as the ester alkylic chain increases, Figures 4a−5a; this trend could be explained considering different factors operating in opposite directions. (i) Liquid structures for alkylbenzoates are characterized by a strong dipolar ordering; as the ester alkylic chain length increases the dipolar moment slightly increases, Figure 6, so this fact should favor a closer packing and thus an increase of density. (ii) The increase of alkylic chain length gives rise to a disruption of the configurational ordering around the ester group because of the dilution of this group with the addition of CH_2 groups, and thus this fact tends to decrease the density. (iii) The loosening of the close packing with increasing alkylic chain decreases the efficiency of dipolar interactions contributing to a decreasing density. Thus, the factors that tend to decrease the density are dominating because the increase of polarity as the alkylic chain increases is very mild and it is not able to balance the factors working in opposite directions. This behavior, in contrast with the increasing density of *n*-alkanes as the chain length increases, has been previously reported for other complex esters[19a] and shows how the liquid structure of aromatic esters is dominated by geometric effects, arising from their size and shape, and by a remarkable dipolar ordering. The decreasing density effect of CH_2 addition is not regular; if data reported in Table S1 of the Supporting Information are analyzed, then we may conclude that the addition of the first CH_2 group (going from MB to EB) causes a density decrease of approximately 3.8% whereas successive additions decrease density by 2.4% (from EB to PB) and 1.5% (from PB to BB) at any of the studied temperatures

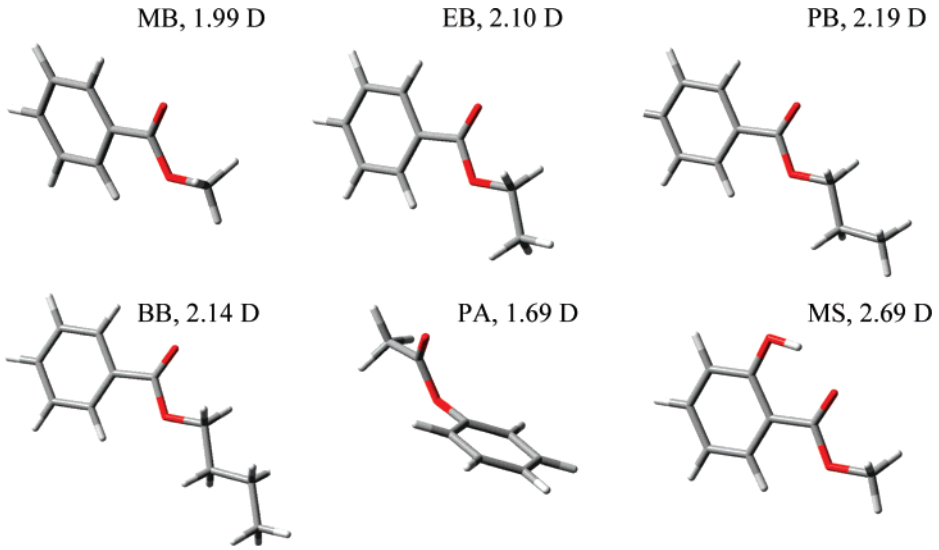

Figure 6. Side views of optimized gas-phase structures of aromatic esters calculated at the B3LYP/6-311++g** theoretical level. Calculated dipole moments are also reported.

and pressures considered; thus the effect of CH_2 seems to be less remarkable as the alkylic chain is longer. Anyhow, the calculated structures of alkylbenzoates reported in Figure 6 show how the planarity of the molecules is not lost as the alkylic chain length increases; this explains the high density of all of the studied alkylbenzoates in spite of the distorting effect of the CH_2 groups on the ester packing. The effect of aromatic ring position with respect to the ester group on density may be analyzed from the results reported in Figures 4a−5a; although the MB density is always higher than that of PA, at any pressure and temperature, the difference between both is very mild: 1.0% at 278.15 K increasing to 1.4% at 358.15 K. In spite of the lower dipolar moment of PA, caused by the electronic delocalization of the ester group through the aromatic ring and its nonplanar shape, Figure 6, this molecule gives rise to an efficient packing that could be explained by considering that the PA shape allows an interpenetration of different packing structures; this fact is confirmed by the remarkably higher viscosity of PA previously reported (1.823 mPa s for MB and 2.421 mPa s for PA at 298.15 K);[11b] the packing of MB is dominated by its planar shape which gives rise to an easier flow in contrast to the interpenetrating PA packing for which a worse flow, higher viscosity, is produced. Finally, the effect of the hydroxyl group's presence on the ester aromatic ring (MS) gives rise to an increase of approximately 8% in density compared with that of MB. This high density could be explained on one hand by the planar shape of MS and on the other hand by its hydrogen-bonding ability; anyhow, both factors operate in the same direction producing a very efficient packing.

The derived properties isobaric thermal expansivity, α_P, isothermal compressibility, k_T, and internal pressure, P_i, were all evaluated by application of well-known relations[17] to the PVT measurements and the TRIDEN fitting coefficients (Table S2); the excellent fitting obtained has enabled a fair description of the PVT behavior; the function put forward is consistent, and the derived properties calculated were fairly accurate.

The reported α_P behavior for aromatic esters is very complex showing several singularities. The common behavior of most fluids is an increasing α_P as the temperature rises along isobars; however the behavior of the studied esters shows the opposite trend for some pressures. In Figure 2b we show how for the high-pressure isobars there is an inflection point from which α_P decreases with increasing temperature; this is confirmed in Figure 3b where a crossing among isotherms implies a change in the $(\partial\alpha_P/\partial T)_P$ function. This trend appears for all of the studied aromatic esters except for MS for which α_P always increases with temperature, Figure 4b and Table S3 of the Supporting Information. This α_P behavior, which is frequently quoted as rare because only some cases such as short alkanols at low temperatures were known,[35a] has been also reported recently for compounds of very different nature such as ionic liquids[35b,d] or even ester oils,[19a] and thus it seems to be not so outstanding as it is confirmed by some molecular simulations.[35d] The density−temperature plots from which the $(\partial\alpha_P/\partial T)_P$ slope is deduced are sometimes very difficult, if not impossible, to calculate because of the very mild deviations from linearity of these functions, and thus sometimes it is difficult to establish $(\partial\alpha_P/\partial T)_P$ values. This is not the case for the aromatic esters studied in this work for two reasons: (i) The use of the TRIDEN fitting function allows the whole description of the fluid's PVT behavior independent of the selection of a particular fitting function for each isobar; (ii) the decrease of α_P is very remarkable, 12% for BB at 60 MPa, well above the error limit, and increases with increasing alkylic chain for alkylbenzoates, Figure 4b. Thus, this anomaly is not a merely mathematical fitting artifact, but it shows highly ordered fluids;[35d] it is surprising that MS does not show the anomaly at any of the studied pressures, which could be justified considering the fluid's hydrogen-bonding structure. However, an increase of alkylic chain length in alkylbenzoate molecules produces a complex α_P behavior; first it increases (on going from MB to EB), and after that it decreases; thus α_P changes in the order EB > MB > PB > BB. The increase in alkylbenzoate chain length gives rise to a lower density and thus to a greater intermolecular free space with increasing capacity to expand or contract; however this does not happen for the studied esters because in the α_P values the two factors operate in opposite directions; as the alkylic chain length increases (i) the density decreases, and thus this fact tends to increase α_P, and (ii) the $(\partial\rho/\partial T)_P$ function decreases, thus tending to decrease fluid compressibility, Figure 7. Thus, for EB a remarkable decrease of density is obtained as aforementioned, and thus this is the dominating fact that gives rise to a greater compressibility compared with that of MB, but for the remaining alkylbenzoates a smaller decrease in density is obtained, and thus the prevailing factor is the decrease in $(\partial\rho/\partial T)_P$, Figure 7, that makes the fluids

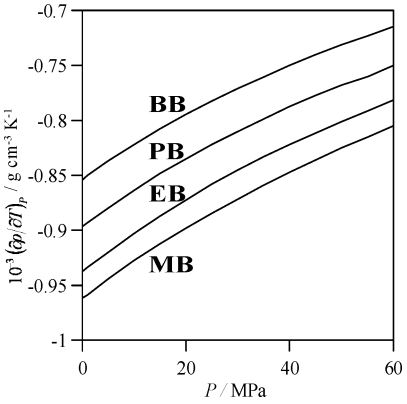

Figure 7. Isothermal variation of density with pressure, $(\partial\rho/\partial T)_P$, at 318.15 K for alkylbenzoates.

less compressible. The $(\partial\rho/\partial T)_P$ function reported in Figure 7 shows smaller values as the alkylic chain increases, which could be related to weaker intermolecular forces in those fluids because of the dilution of the ester group. PA is the most compressible fluid among the studied esters because its shape gives rise to a packing that in spite of being efficient, as is shown by its density, has more free volume than the remaining esters. MS gives rise to the lower α_P values, the high-density values of this fluid point to a highly structured liquid because of the hydrogen-bonding ability, and the $(\partial\rho/\partial T)_P$ values are the higher ones among the studied esters, showing that ordering through intermolecular interaction is highly remarkable.

The behavior of k_T shows the regular trends for all of the studied esters, increasing with temperature along isobars and decreasing with pressure along isotherms, Figures 2c−5c, because of the diminution of free space as pressure rises or temperature decreases. The $(\partial\rho/\partial p)_T$ term that decreases with increasing pressure or decreasing temperature, Figures 2c−3c, determines the trends of k_T. The values reported for the studied esters are small, and thus these fluids are only slightly compressible, MS being the least compressible one. The strong pressure and temperature effects on k_T show again highly structured fluids.

Internal pressure, reported in Figures 2d−5d, is defined as $P_i = (\partial U/\partial V)_T$ and represents the work exerted against the cohesive forces by a liquid that undergoes an isothermal expansion entailing a change in internal energy.[36] This property is related to the cohesive energy density, c, and the two properties are approximately equal for weakly polar fluids whereas there is an increasing difference among both ones as specific or stronger dipolar interactions appear in the fluid. The Hildebrand solubility parameter, δ, is a very important property for different applications and is defined as $c^{0.5}$; this property is not easily experimentally available, mainly at high pressures, and its determination is commonly done at atmospheric pressure through vaporization enthalpy measurements. Thus, if a relationship could be established among the P_i and δ values, then this would be very valuable for many solubility applications. In Table 1 we report a comparison among experimental δ values and those calculated directly from P_i; so-called experimental values were calculated according to the group contribution procedure reported by Hansen[37] because δ parameters are not available in the literature for all of the studied esters from reliable sources, and thus to allow a fair comparison all of them were calculated with this reliable method. The results show how for alkylbenzoates δ parameters could be calculated with enough accuracy through P_i values, and thus this property could be used to determine the value of this parameter at higher temperatures and/or pressures. MS shows different results; the experimental value is remarkably higher than the calculated one because of the strong intermolecular forces. We may define according to Dack[36] energies arising from nonchemical weak interactions (those present in fluids with $\mu < 2$ D), E_0, and those arising from stronger forces (hydrogen bonding and strong dipolar interactions), E_1

TABLE 1: Hansen Solubility Parameters, δ, and Energy Contributions Defined According to Eqs 5 and 6, E_0 and E_1, for Aromatic Esters at 298.15 K

compound	δ_{EXP}/MPa$^{0.5}$ [a]	δ_{P_i}/MPa$^{0.5}$ [b]	E_0/kJ mol^{-1}	E_1/kJ mol^{-1}
MB	20.8	21.0	55.7	−1.3
EB	20.3	20.2	58.6	0.8
PB	19.9	19.8	63.9	0.5
BB	19.7	19.6	68.2	0.9
PA	20.7	21.3	57.9	−3.4
MS	25.5	21.4	59.0	25.1

[a] Calculated according to the group contribution procedure reported in ref 37. [b] Calculated as $\delta_{P_i} = P_i^{0.5}$.

$$E_0 = \frac{P_i M}{\rho} \tag{5}$$

$$E_1 = \frac{(c - P_i)M}{\rho} \tag{6}$$

The strong E_1 term for MS arises from the remarkable dipolar moment, Figure 6, of this molecule together with its hydrogen-bonding ability. For the remaining aromatic esters E_1 is almost null, but the E_0 term is important pointing to efficient dipolar interactions among molecules. Anyhow, the P/T behavior of P_i is complex, Figures 2d−5d; at low temperatures P_i increases slightly with increasing pressure, but the trend is inverted at high temperatures with a stronger pressure effect; along isobars a maximum appears for all of the studied esters. These features justify the α_P anomaly and in general are related to an important fluid ordering mainly through dipolar interactions.

Equations of State. The predictive abilities of SAFT[15] and PC-SAFT[16] molecularly based EOS's were tested in this work. The EOS characteristics and equations may be found in the original papers, and thus they are not described here for the sake of brevity. The terminology used for the different model parameters agrees with that used in the original EOS works.[15,16] Aromatic ester SAFT and PC-SAFT parameters are not available in the literature, so they were obtained from simultaneous correlation of saturation pressures and saturated liquid densities according to a least-squares procedure. Saturated liquid density literature data were unavailable for some of the studied esters, and they were calculated under P/T saturation conditions using the TRIDEN parameters reported in Table S2 of the Supporting Information. For MS two association schemes were considered, the rigorous three sites (3B) and the simplified two sites (2B). The parameters obtained in this way were used to predict the PVT properties of the studied esters.

Results from saturation property correlations are reported in Table S6 of the Supporting Information. PC-SAFT provides better correlations than the SAFT EOS for almost all of the studied compounds; this is more remarkable for saturation density predictions for which the quality of the PC-SAFT correlations is higher. Saturation pressures are correlated successfully by both models although deviations are higher at low or high temperatures, Figure 8. A comparison of the correlation quality in the vicinity of the critical point cannot be done because of the absence of reliable data for most of the compounds;

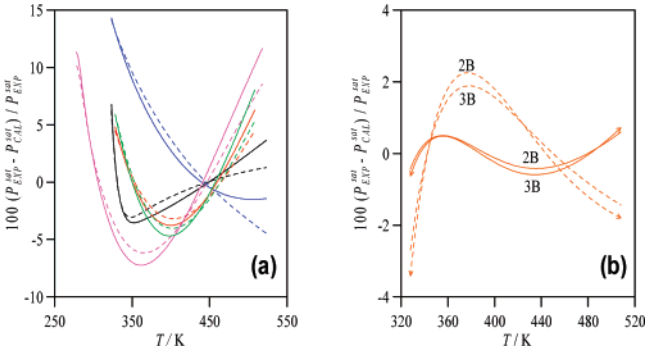

Figure 8. Percentage errors in the calculated vapor pressure for aromatic esters: (black) MB; (blue) EB; (red) PB; (pink) BB; (green) PA; (orange) MS. Continuous lines represent SAFT, and dashed lines PC-SAFT. Association schemes are indicated for MS. Parameters are from Table S2 of the Supporting Information.

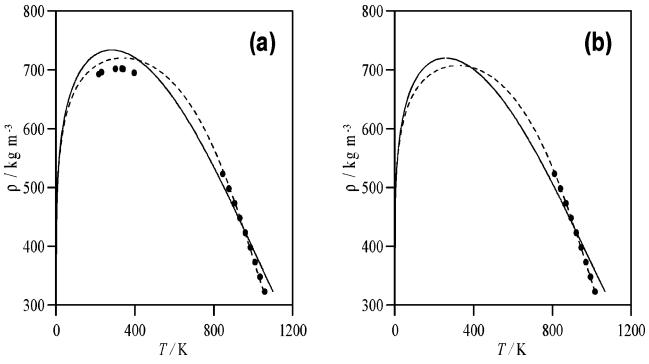

Figure 9. Saturation dome for (a) MB and (b) EB: (●) experimental;[38] (—) SAFT; (---) PC-SAFT. Parameters are from Table S2 of the Supporting Information.

anyhow, although both models overpredict the critical points, Table S6 of the Supporting Information, like for any mean field approach, results are better for PC-SAFT as shown in Figure 9 for MB. Results for MS are of a lower quality than those for the remaining esters with both EOS's; although MS vapor pressure is surprisingly well correlated by SAFT model, both EOS's give rise to high deviations in saturation density although results are slightly better for PC-SAFT. This is clearly caused by the strong intermolecular forces, hydrogen bonding and strong dipolar interactions, present in fluid MS. The application of these EOS's to self-associative compounds such as MS requires the a priori selection of the association scheme; for MS two possible options are available: a rigorous three-site model considering the two lone electron pairs of oxygen and the proton, both in the hydroxyl group (3B according to the SAFT terminology)[15] and a simplified two-site model, in which only one electron pair is considered (2B).[15] Both possibilities were studied in this work, Table S6 of the Supporting Information and Figure 8, and from the results we may conclude that correlation qualities are almost unaffected by the association model. Anyhow, the association parameters of both EOS's have a clear physical meaning because they are related to the enthalpy and entropy of hydrogen bonding;[42] thus, on one hand, the value of these parameters must be kept within certain limits during the correlation procedure to obtain parameters with physical sense (although better correlations could be obtained with other parameters through a purely mathematical fitting but losing their physical meaning), and on the other hand, information about the hydrogen-bonding strength may be inferred from the EOS fitting. Enthalpy, Δh^{HB}, and entropy, Δs^{HB}, of association calculated according to the procedure of Gupta et al.[42] from model parameters are reported in Table 2; results obtained with

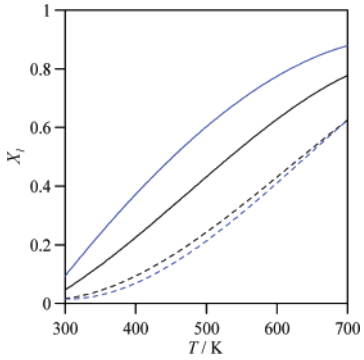

Figure 10. Monomer fraction in liquid MS at saturation for the SAFT and PC-SAFT EOS's with different association models: (black solid line) SAFT/2B; (black dotted line) SAFT/3B; (blue solid line) PC-SAFT/2B; (blue dotted line) PC-SAFT/3B. Parameters are from Table S2 of the Supporting Information.

TABLE 2: MS Enthalpies, Δh^{HB}, and Entropies, Δs^{HB}, of Association Calculated According to the Procedure of Gupta et al.[42] from EOS Parameters Reported in Table S6 of the Supporting Information

	SAFT		PC-SAFT	
	$-\Delta h^{HB}$/kJ mol^{-1}	$-\Delta s^{HB}$/J mol^{-1} K^{-1}	$-\Delta h^{HB}$/kJ mol^{-1}	$-\Delta s^{HB}$/J mol^{-1} K^{-1}
2B	14.0	32.4	13.1	30.7
3B	12.3	36.3	14.3	35.4

both EOS's are very similar with strong hydrogen-bonding energy and remarkable entropic effects arising from the planar shape of MS. No experimental spectroscopic data on MS hydrogen-bonding strength are available to compare with those calculated through the EOS analysis. However, the E_1 energy previously obtained from the internal pressure analysis is clearly greater than any of the Δh^{HB} values obtained, and thus a strong contribution from the dipolar interactions (~11 kJ mol^{-1}) appears in this fluid. However, molecularly based EOS parameters for self-associative compounds allow the calculation of the monomer fraction in the fluid, that is to say, fraction of non-hydrogen-bonded molecules, for different temperatures and pressures. The monomer fraction, X_1, may be obtained experimentally,[43] although no results are available for MS, and thus comparison with the EOS predictions is not possible. Anyhow, X_1 was calculated to obtain a deeper insight into the fluid structure with SAFT and PC-SAFT and both association models considering that it is the product over all M sites of the fraction of molecules not bonded at each site A, X^A, eq 7,[44] where this fraction comes from the procedure proposed by Huang and Radosz[15b] from the model association parameters and the selected association schemes

$$X_1 = \prod_{A=1}^{M} X^A \tag{7}$$

In Figure 10, we report the MS calculated values of X_1 for the saturated liquid according to both EOS's studied and the association schemes. Remarkable differences are obtained among three- and two-site results, with a much higher fraction of free MS molecules for this last scheme. However, the simultaneous interaction with the two lone pairs of the hydroxylic group seems to be sterically hindered because of the voluminous aromatic ring, and thus the two-site model is probably more realistic. Anyhow, at temperatures close to the ambient conditions MS shows strong interactions through

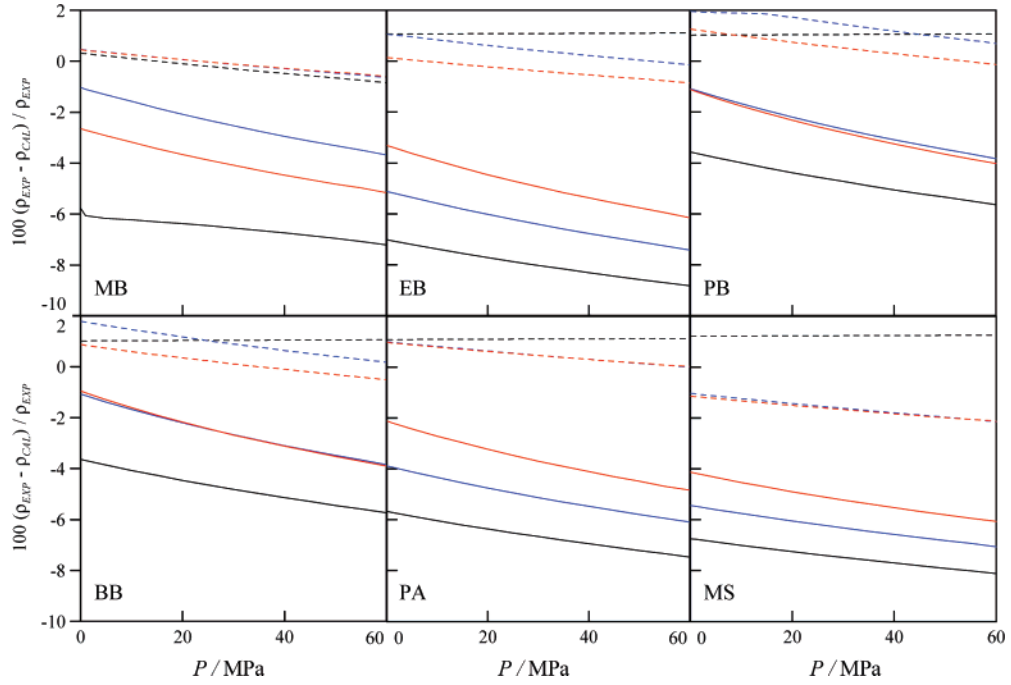

Figure 11. Percentage errors in the calculated compressed liquid densities for aromatic esters at different isotherms: (black lines) 278.15 K; (blue lines) 318.15 K; (red lines) 358.15 K. Continuous lines represent SAFT, and dashed lines PC-SAFT. The 2B association scheme is for MS with both EOS's. Parameters are from Table S2 of the Supporting Information.

TABLE 3: B3LYP/6-311++g Optimized Geometries and Charges in the Gas Phase and Solution (IEF-PCM Approach) of Aromatic Esters**[a]

	MB	MB_{sol}	EB	EB_{sol}	PB	PB_{sol}	BB	BB_{sol}	PA	PA_{sol}	MS	MS_{sol}
$C{=}O_c$	1.210	1.212	1.211	1.214	1.211	1.214	1.211	1.214	1.200	1.203	1.227	1.229
$C{-}O_a$	1.352	1.347	1.350	1.346	1.350	1.346	1.350	1.346	1.372	1.369	1.342	1.337
$C_a{-}C$	1.491	1.492	1.492	1.493	1.492	1.493	1.492	1.493			1.471	1.472
$O_h{-}C_a$											1.345	1.349
$\angle O_c{-}C{-}O_a$	122.9	123.1	123.1	123.3	123.2	123.4	123.2	123.4	124.0	124.2	121.8	122.1
$\phi(C_a{-}C_a{-}C{-}O_c)$	0.0	0.0	0.0	0.0	0.0	0.0	0.0	0.0			0.0	0.0
$\phi(O_c{-}C{-}O_a{-}C_m)$	0.0	0.0	0.0	0.0	0.0	0.0	0.0	0.0			0.0	0.0
$\phi(C{-}O_a{-}C_a{-}C_a)$									60.6	60.7		
$\phi(O_h{-}C_a{-}C_a{-}C)$											0.0	0.0
$\phi(H_O{-}O_h{-}C_a{-}C_a)$											0.0	0.01
O_c	−0.531	−0.546	−0.602	−0.617	−0.616	−0.630	−0.605	−0.620	−0.558	−0.573	−0.594	−0.613
C	0.689	0.700	0.865	0.876	0.950	0.961	0.925	0.936	0.889	0.901	0.802	0.813
O_a	−0.285	−0.260	−0.464	−0.461	−0.524	−0.501	−0.410	−0.388	−0.515	−0.492	−0.278	−0.250
O_h											−0.682	−0.699
H_O											0.482	0.481
C_m	−0.166	−0.160	0.349	0.352	0.213	0.217	0.018	0.016			−0.208	−0.200

[a] Bond lengths are in ångstroms, and angles are in degrees. C = ester carbon; O_c = carbonyl oxygen; O_a = alkoxy oxygen; C_a = aromatic carbon; C_m = carbon bonded to O_a; O_h = hydroxyl oxygen; H_O = hydroxyl hydrogen.

hydrogen bonding, and most of the molecules are bonded although as the temperature rises this fraction decreases remarkably.

The EOS's ability for prediction of compressed liquid densities is analyzed in Figure 11. From the reported results we may conclude that PC-SAFT predictions are remarkably more accurate than SAFT ones including for the self-associative MS fluid. The deviations increase as pressure rises and decrease with increasing temperature with both models. Hence, PC-SAFT describes adequately the aromatic ester properties in the *P*/*T* range considered whereas SAFT should be discarded for these systems.

Quantum Calculations. The DFT-optimized structures of aromatic ester monomers calculated in the gas phase at the B3LY6-311++g** theoretical level are reported in Figure 6, and the main geometrical parameters and charges in Table 3. The aforementioned planarity of alkylbenzoate molecules is the most remarkable attribute of these molecules; this planarity is not lost as the alkylic chain length increases to keep the resonance energies in their optimal values by the delocalization of the π-electron system through the ester group.[45] The torsional barrier around the bond joining the aromatic ring and the ester group, $\phi(C_a{-}C_a{-}C{-}O_c)$ was calculated through relaxed scanning of the potential energy surfaces (PES's) at 10° intervals at the B3LYP/6-311++g** theoretical level. With this procedure, for each change of the torsional angle, the structure is fully optimized for that fixed angle, thus relaxing the remaining degrees of freedom. Results reported in Figure 12 show how the barrier is almost independent of the alkylic chain length; only a slight decrease is produced on going form MB to BB. The maxima in the PES scanning produced at 90°, ∼6.4 kcal mol^{-1}, may be identified with the resonance energy. These results are concordant with experimental structural X-ray data.[46] The main geometric parameters reported in Table 3 are almost unaffected by the increasing length of the alkylic chain; only MK charges of the ester group atoms change; hence, the

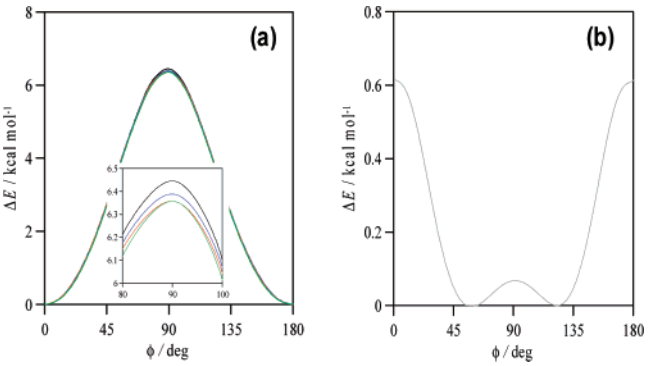

Figure 12. Calculated relaxed potential energy scanning for the dihedral angle (a) $\phi(C_a-C_a-C-O_c)$ of alkylbenzoates and (b) $\phi(C-O_a-C_a-C_a)$ of PA, calculated at the B3LYP/6-311++g** theoretical level: (black) MB; (blue) EB; (red) PB; (green) BB; and (light black line) PA

carbonyl, O_c, and alkoxy, O_a, oxygens are more negative as the chain length increases as the ester carbon, C, is more positive. The calculated MK charges were used for the molecular dynamics simulations.

The torsional profile reported for PA around the $\phi(C-O_a-C_a-C_a)$ dihedral angle, Figure 12b, is completely different; in spite of the minimum conformation at 60.6°, Figure 6 and Table 3, a very small barrier of ~0.6 kcal mol^{-1} is reported, and thus PA can evolve from planar to nonplanar structures almost freely. These values are consistent with values previously reported through X-ray structural data[46] or lower theoretical levels[47,48] and are independent of the chemical group forming the ester, as is shown by experimental and calculated results reported for phenylbenzoate.[49,50]

The strong effects of ortho substituents on the rotational barriers of aromatic esters are well-known.[45] The presence of ortho hydroxyl groups in benzoates is especially important because of the possible formation of intramolecular hydrogen bonding among the hydroxylic hydrogen and any of the ester oxygens. Four possible planar conformers are considered in this work, Figure 13; in a similar way to those reported for salicylic acid,[51,52] conformers MS1 and MS2 allow the formation of intramolecular hydrogen bonding whereas MS3 and MS4 do not allow it. Transitions among the different conformers may be done through torsions around the $\phi_1(C_a-C_a-C-O_c)$ and $\phi_2(H_O-O_h-C_a-C_a)$ angles. The order of stability (increasing energy) is MS1 > MS2 > MS4 > MS3, Figure 13; thus, strong intramolecular hydrogen bonding is produced in MS, as is confirmed through spectroscopical results.[53] The MS2 conformer, in which hydrogen bonding is also present, shows a higher energy than that of MS1, and the evolution from MS1 to MS2 is done through a remarkable barrier. The strength of hydrogen bonds may be calculated as the difference among the open and closed conformers, MS1 with MS3 and MS2 with MS4, obtaining values of 11.52 kcal mol^{-1} for MS1 and 7.97 kcal mol^{-1} for MS2. Anyhow, the rotation among any of the considered torsional angles is not free, and thus MS1 must be considered as the predominant conformer. The hydrogen bond lengths reported in Figure 13 are short, which would justify the formation of the cyclic intramolecular structure as previously reported for salicylic acid.[51,52]

Although the study of monomer properties, that is to say gas phase behavior, is of remarkable importance because of the supplied information, the description of liquid-phase properties requires the study of wide collections of molecules interacting among themselves. The study through quantum methods of properties for large collectives of molecules is not feasible at this moment because of the enormous computational resources required; thus, the so-called supramolecular approach has to be limited to a small number of molecules. In spite of these limitations, we have computed the energy of a MB cluster formed by five molecules to study the efficiency of intermolecular interactions through dipolar interactions, Figure 14. Interaction energy, ΔE, was calculated as the difference among the cluster and monomer energies at the B3LYP/6-311++g** level with the basis set superposition error (BSSE) corrected through the counterpoise procedure.[54] The results reported in Figure 14 show a very efficient molecular packing with a remarkable interaction energy arising from the interaction among the dipolar moments, although these results must be analyzed with caution; because of the small number of molecules involved, they would justify the aforementioned thermophysical properties of MB. In an analogous way, we have done calculations on MS dimers to explore the intermolecular hydrogen-bonding ability of this molecule in the gas phase; several positions were analyzed, and results are reported in Figure 15. The dimers reported in Figure 15 show that although intermolecular hydrogen bonding is possible, as the short distances point to, the energy of these interactions is very small. These low energies point to a dynamic hydrogen-bonding network in which these interactions are easily formed and destroyed; this will justify the previous EOS monomer fraction analysis from which most of the MS molecules were hydrogen-bonded at ambient temperature. Anyhow, the intermolecular interaction through the carbonyl oxygen position is clearly favored, dimers 2MS1 and 2MS2 in Figure 15, whereas the interaction through the alkoxy oxygen should be discarded, 2MS3 in Figure 15.

Another approach to study the behavior of liquid phases is through the use of solvation continuum models, in which the interaction among a monomer or a cluster and a surrounding solvent, that has lost its molecular nature replaced by a structureless description. The continuum models diminish the complexity of the computational problem but provide valuable information on polarization and long-range effects. Thus, in this work we have studied the behavior of aromatic ester monomers solvated by surrounding solvents whose characteristics are those of the respective esters. The continuum solvation model is represented by the integral equation formalism version of the polarizable continuum model (IEF-PCM).[55] Ester parameters required for IEF-PCM calculations are reported in Table S7 of the Supporting Information, and results in Table 3. Very mild differences among gas phase and IEF-PCM results are obtained; thus a weak effect of the surrounding medium is obtained; the geometrical features and the orientational facts that characterize the interaction among dipolar aromatic ester molecules are not properly represented by the continuum model. The electrostatic potentials (ESPs) are shown in Figure 16 for all of the studied esters in the gas phase; results in solution according to the IEF-PCM approach are not reported because negligible changes occur for all of the studied compounds. For alkylbenzoates, the negative charge is concentrated on the carbonyl oxygen whereas the alkoxy oxygen shows less remarkable charge. For MB, the methyl hydrogens show remarkably positive charges that decrease as the chain length increases to BB. PA shows a complex charge distribution with negative charge on the carbonyl oxygen, but the nonplanar shape of this molecule hinders the interaction among the carbonyl and phenyl charge distributions. Finally, MS shows a strong region of negative charges in the hydroxyl and carbonyl oxygens together with a positive charge in the hydroxyl hydrogen in the neighborhood

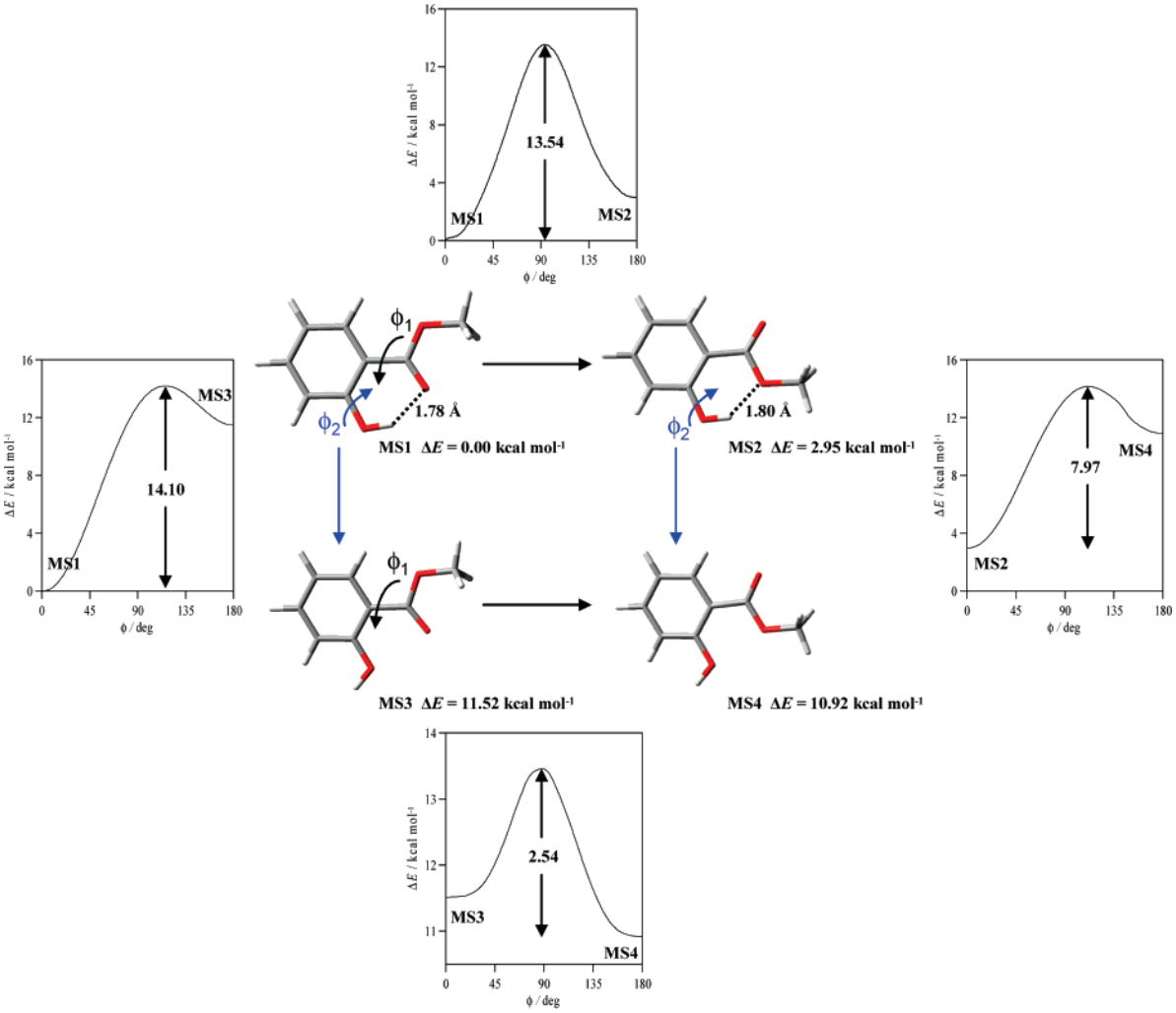

Figure 13. Conformers, torsional barriers and relative energies, ΔE, of MS in the gas phase calculated at the B3LYP/6-311++g** theoretical level. All ΔE values are referred to the MS1 conformer.

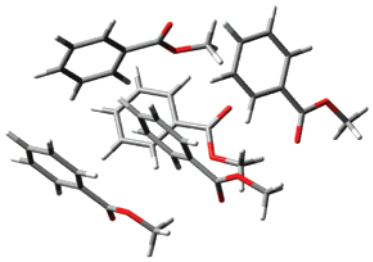

Figure 14. Optimized structure and interaction energy, ΔE (BSSE counterpoise corrected), at the B3LYP/6-311++g** theoretical level for a cluster formed by five MB molecules

of the oxygen giving rise to the strong intramolecular hydrogen bonding. For MS, methyl hydrogens show a less positive charge in comparison with those obtained for MB.

Molecular Dynamics Simulations. Molecular level information about the structure of liquid aromatic esters may be inferred from molecular dynamics (MD) studies. The NPT MD results obtained in this work also allow us to obtain theoretical values of important thermophysical properties that may be compared with the experimental accurate values reported.

Structural information on fluid structure is commonly analyzed through radial distribution functions (RDFs). RDFs for alkylbenzoates are reported in Figure 17 for selected atomic pairs. The interaction among neighboring COO groups is characterized by a first peak in RDFs around 5 Å ($C-O_c$, $C-O_a$, and O_c-O_a) with decreasing intensity as the alkylic chain length increases; although its position remains almost constant, the integration of these first peaks up to the first valley gives a value of 2.7 molecules in this first coordination shell for MB that decreases to 2.1 for BB. The interaction among the apolar alkylic chains (C_m-C_m) is characterized by a complex RDF behavior, a first peak at 4.1 Å disappearing as the alkylic chain increases with a new maxima appearing at 5.1 Å; from the RDFs reported it seems clear that alkylic chains remain close in the fluid structure, as is shown by the sharp peaks in the RDFs, probably giving rise to continuous apolar domains in the liquid esters. The interaction of carbonyl oxygen, O_c, with the different hydrogens available in the molecules is clearly different from those of alkoxy oxygens, O_a. The interaction of O_c with the hydrogens in the aromatic ring is characterized by a remarkable first peak, although not very intense, at 2.8 Å; although the intensity of this peak first decreases on going from MB to EB and after that it increases, its positions are unaffected by the type of alkylbenzoate considered, and it may point to a possible weak hydrogen bonding between the carbonyl oxygen and the aromatic ring. Surprisingly, another sharp peak appears for the O_c-H_m pairs also at 2.8 Å; the effect of alkylic chain length on this peak is very remarkable, decreasing very quickly from MB to BB; the vicinity of the methyl group to the highly polar ester group may favor the interaction between the hydrogens of this group (with remarkable positive charges, Figure 16) and

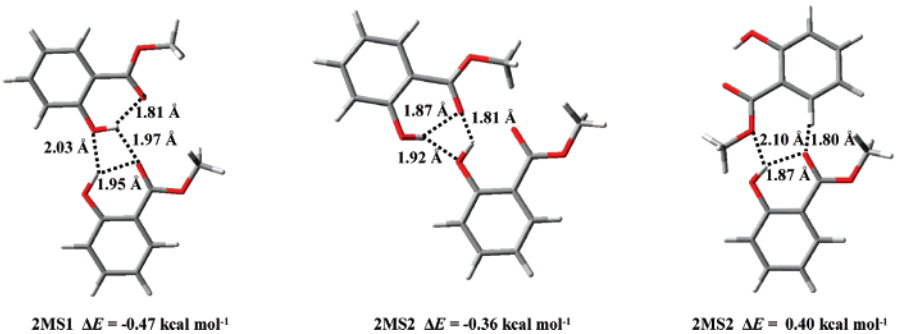

Figure 15. Optimized MS gas-phase dimers calculated at the B3LYP/6-311++g** theoretical level for three different positions, where ΔE is the interaction energy (BSSE counterpoise corrected). Interatomic distances for possible hydrogen bonding are also reported.

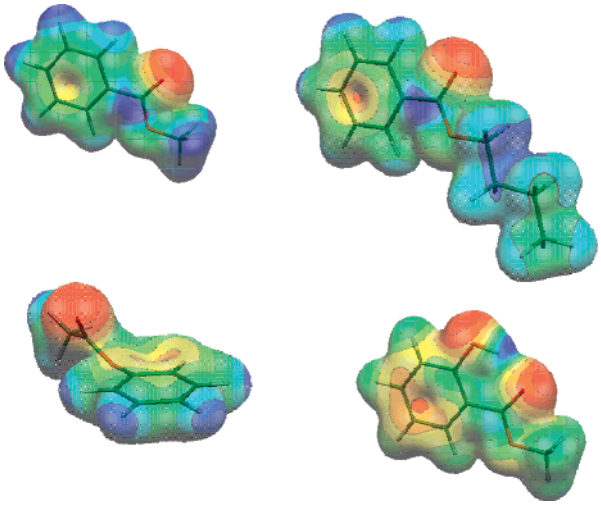

Figure 16. Gas-phase electrostatic potential surfaces mapped on an electronic density surface isovalue of 0.0004 a.u., calculated at the B3LYP/6-311++g** theoretical level. Color scale: blue, positive; red, negative.

the neighboring carbonyl oxygens, whereas as the alkylic chain length increases the hydrogens of the alkylic chains may lose their capacity to interact with the oxygen; from the RDFs an unusual weak hydrogen bond between the carbonyl oxygen and the methyl hydrogen may be inferred; the integration of this first peak for MB up to the first valley gives a value of 1.5 molecules in this first solvation shell. This interaction should be discarded for the alkoxy oxygens for which peaks at approximately 5 Å are obtained.

Dynamic properties are important quantities, not easily measurable, to characterize fluids. The self−diffusion coefficient, D, may be calculated from Einstein's relation

$$D = \frac{1}{6}\lim_{t\to\infty}\langle \Delta r(t)^2 \rangle \qquad (8)$$

where the quantity in brackets, the mean-square displacement (MSD), is plotted in Figure 18 for the first 30 ps of the simulation after equilibration with a linear behavior for longer times. The slope of the linear fittings of the MSDs gives rise to the D values reported in Table 4; decreasing values of D are obtained as the alkylic chain length increases; this is in agreement with the increasing values of viscosity on going from MB to BB[11f] as the Stokes−Einstein equation shows. Anyhow, although as far as we know, no experimental D values are available for alkylbenzoates, and thus comparison is not possible; the calculated values seem to be reasonable and reflect the fluid structure with weaker intermolecular forces as the chain length increases.

The strength of the intermolecular forces may be inferred from an analysis of the energies of the liquid, E_{LIQ}, and the gas phase, E_{GAS} (in which intermolecular forces are almost negligible), simulations; thus this intermolecular energy may be equal to $E_{GAS} - E_{LIQ} + RT$; results of these calculations are reported in Table 5. The intermolecular energy decreases as the alkylic chain length increases, and the results obtained are very close to experimental vaporization enthalpies (13.28 kcal mol^{-1} for MB).[57]

Another important use of MD simulations is the prediction of thermophysical properties. NPT density predictions obtained in this work are compared with experimental values for alkylbenzoates in Figure 19 at 298 K and 0.1 MPa; an excellent agreement is obtained for the four studied esters with the greater deviations for MB but with errors lower than 1% for all of the studied compounds. These accurate predictions, on one hand, show how OPLS-AA is an adequate force field to describe alkylbenzoate properties and, on the other hand, show that MD simulations capture the main structural features of these fluids. Although additional MD simulations should be done at higher pressures and temperatures, which will be done in future works, and thus these results should be considered as preliminary; this method seems to be remarkably accurate for these fluids.

MD results for PA are reported in Figure 20; the position of the phenyl group with respect to the ester group has remarkable effects on RDFs if MB and PA results are compared. The interaction among the ester groups is weakened in PA, as is showed by the C−O_c and O_c−O_a RDFs; this may be explained considering the nonplanar shape of PA in which the interaction among neighbor groups is sterically hindered. On the contrary the aforementioned possible hydrogen bonding between the carbonyl oxygen and the aromatic ring hydrogens is reinforced with a more intense peak although the position is unaffected on going from MB to PA. The PA self-diffusion coefficient of PA is surprisingly remarkably higher than that of MB, Table 4, but this is concordant with the lower intermolecular energy reported in Table 5. Thus, although the interaction between the ester group and the aromatic ring is favored in PA at the same time the interaction with the polar ester group is disfavored and considering that this last fact is quantitatively more important, intermolecular forces are weakened as a whole. The MD-predicted density for PA at 298 K and 0.1 MPa is 1.1420 g cm^{-3}; this value is 6.7% higher than the experimental one reported in Table S1 of the Supporting Information; thus MD simulations do not capture accurately the liquid PA structural features; these may be produced by the low torsional barrier reported in Figure 12 that may give rise to an almost free rotation of the ester group with the complex effects on the behavior of the intermolecular forces.

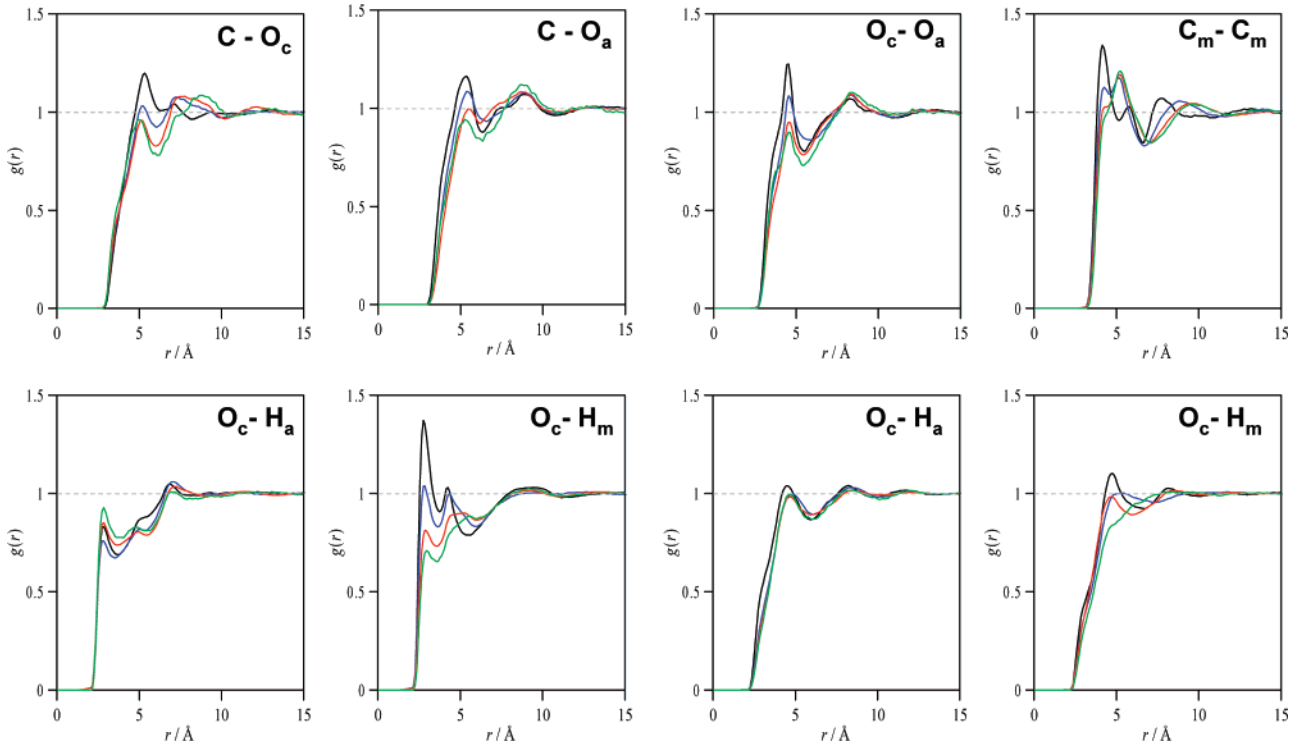

Figure 17. Radial distribution functions, $g(r)$, for liquid-phase alkylbenzoates at 298 K and 0.1 MPa: (black) MB; (blue) EB; (red) PB; (green) BB; r = interatomic distance; C = ester group carbon, O_c = carbonyl oxygen; O_a = alkoxy oxygen; C_m = terminal carbon of the alkylic chain; H_a = hydrogens in the aromatic ring; H_m = hydrogens in the terminal carbon of the alkylic chain.

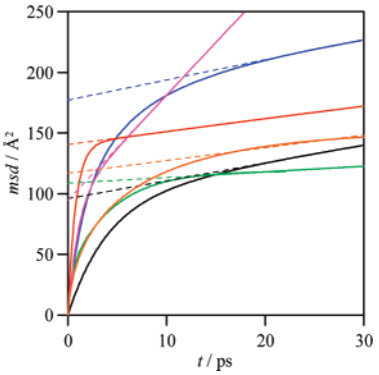

Figure 18. Mean-square displacement for aromatic esters for the first 30 ps of molecular dynamics simulations after equilibration at 298 K and 0.1 MPa. MSDs are represented by continuous lines, and dashed lines represent the linear regime used for the calculation of self-diffusion coefficients according to Einstein's relation: (black) MB; (blue) EB; (red) PB; (green) BB; (pink) PA; (orange) MS.

TABLE 4: Calculated Self-Diffusion Coefficients, *D*, at 298 K and 0.1 MPa for the Aromatic Esters from MSD Plots According to Einstein's Relation in the Time Intervals Where Linear Regime is Reached

	MB	EB	PB	BB	PA	MS
$10^9\ D/m^2\ s^{-1}$	2.09	2.19	1.70	0.80	14.05	1.74

TABLE 5: Intermolecular Energy, Calculated as $E_{GAS} - E_{LIQ} + RT$, for the Aromatic Esters from NPT Molecular Dynamics Simulations at 298 K and 0.1 MPa

	MB	EB	PB	BB	PA	MS
$E_{GAS} - E_{LIQ} + RT$/kcal mol^{-1}	13.02	10.44	9.59	7.13	8.60	15.02

The structure of liquid MS is characterized by hydrogen bonding of an intra- and intermolecular nature. We have showed previously that intramolecular hydrogen bonding is present in MS, but although intermolecular hydrogen bonding is also

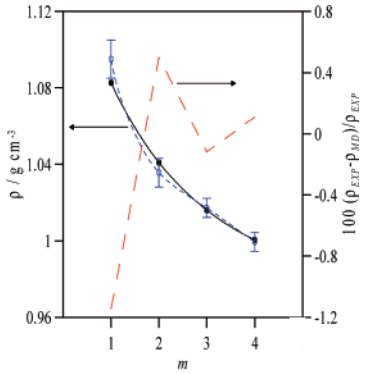

Figure 19. Experimental (●, Table S1 of the Supporting Information) and calculated (○, OPLS-AA NPT molecular dynamics) densities for alkylbenzoates as a function of carbon atoms in the alkylic chain, m, at 298 K and 0.1 MPa. Error bars for calculated densities and percentage error (red dotted line) are also reported.

present the energy of this interaction is very weak in all of the studied positions, Figure 15. RDFs for selected atomic pairs are reported in Figure 21 for the O_h-H_o pair, which shows the interaction between neighboring hydroxylic groups; a sharp peak at 2.0 Å is obtained; this distance is concordant with that previously obtained from DFT calculations and is characteristic of hydrogen bonding; however, this peak is not very intense, and its integration up to the first valley gives a value of 1 molecule in this shell. Thus, although the interaction between neighboring hydroxyl groups is present, this is clearly weak, and thus very dynamic, probably because the strong intramolecular hydrogen bonding hinders the simultaneous interaction with other molecules. Another possible hydrogen bond may be established between the hydrogen of the hydroxylic group and the carbonyl oxygen, although the RDF for this pair (excluding intramolecular pairs) shows a peak at 2.0 Å (in agreement with DFT results, Figure 15); this peak is not very intense, integrating to 1 molecule (because the minima appears at greater distances

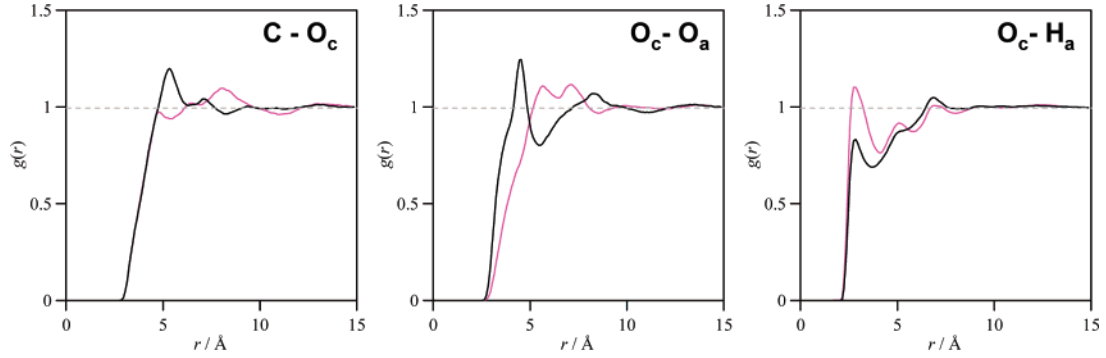

Figure 20. Radial distribution functions, $g(r)$, for liquid-phase MB and PA at 298 K and 0.1 MPa: (black) MB; (red) PA; r = interatomic distance; C = ester group carbon; O_c = carbonyl oxygen; O_a = alkoxy oxygen; H_a = hydrogens in the aromatic ring.

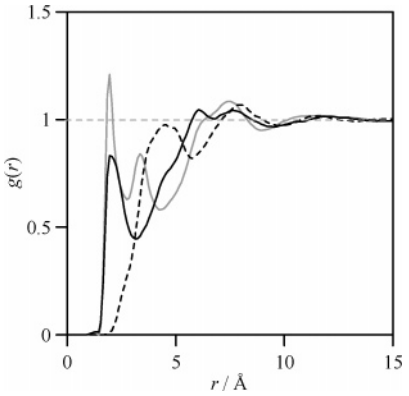

Figure 21. Radial distribution functions, $g(r)$, for liquid-phase MS at 298 K and 0.1 MPa: (gray solid line) O_h-H_O; (black solid line) H_O-O_c; (black dotted line) H_O-O_a; r = interatomic distance; O_h = hydroxyl oxygen; H_O = hydroxyl hydrogen; O_c = carbonyl oxygen; O_a = alkoxy oxygen. We should remark that for H_O-O_c, as for other pairs, intramolecular pairs are not included.

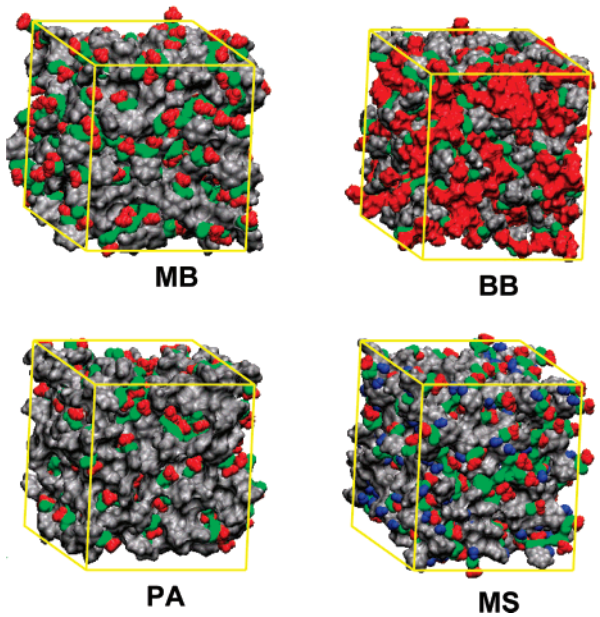

Figure 22. Snapshots of liquid-phase aromatic esters obtained from NPT molecular dynamics simulations at 298 K and 0.1 MPa. Color code for different domains: (gray) aromatic rings; (green) COO groups; (red) alkylic chains; (blue) OH group in MS.

than for the O_h-H_o pair, showing a bigger shell). The interaction between the alkoxy oxygen and the hydroxylic hydrogen should be discarded as the DFT results showed. Thus, although MS has the ability to develop intermolecular hydrogen bonding, this is clearly hindered by the presence of intramolecular hydrogen bonds among the hydroxyl and carbonyl oxygen groups. The self-diffusion coefficient for MS is lower than that for MB because of its greater viscosity.[58] The energy values reported in Table 5 show that the intermolecular hydrogen-bonding contribution is very small as the DFT results showed. MD simulations for MS predict a density value at 298 K and 0.1 MPa of 1.1902 g cm^{-3}, which is only 1.2% greater than the experimental value reported in Table S1 of the Supporting Information.

Finally, in Figure 22 we show MD representative snapshots for the studied aromatic esters. For the analysis of fluid structure, a color code was used to distinguish among the different molecular parts. The molecular structrure was divided into three different regions: aromatic ring, ester group, and apolar alkylic chain. An additional region corresponding to the hydroxyl group was considered for MS. For MB a region formed by phenyl rings extends along the fluid being permeated by ester and methyl groups; as the alkylic chain length increases an apolar domain formed by these chains extends in the fluid dominating the fluid structure. Thus, for MB, interaction between the ester group and the remaining molecular parts is possible, but for BB this interaction is hindered, and the fluid structure is dominated by apolar alkylic domains. This is in agreement with the aforementioned RDF behavior. If we compare the MB and PA fluid structures reported in Figure 22, then no large differences are obtained, but it seems that in PA the aromatic domains are better interconnected as previous RDF results showed. The MS structure is very close to that for MB; the hydroxyl groups are disperse in the fluid, and thus not a clear intermolecular hydrogen-bonding network may be deduced; hence, the structure is again dominated by aromatic domains permeated by the ester groups.

Concluding Remarks

This work reports on a combined experimental and theoretical study on the structure and properties of aromatic esters. The fluid behavior reveals a number of anomalies related to the structural fluid complexity, such as a falloff of α_P values with rising temperature along isobars. The modeling of PVT behavior with state-of-the-art EOS's is not accurate enough, and only PC-SAFT gives rise to good predictions whereas SAFT should be discarded for these fluids. The theoretical study shows the existence of a remarkable structural ordering of a dipolar nature; although unusual weak hydrogen bonding between the carbonyl group and the aromatic hydrogens and/or alkylic hydrogens is also possible mainly for short chain benzoates. For MS the intramolecular hydrogen bonding hinders the formation of intermolecular interactions that although are present are very weak and dynamic. For PA the almost free rotational barrier

gives rise to a complex fluid structure. The molecular dynamics study according to the OPLS-AA force field provides a reliable description of the fluid structure and an efficient tool to predict aromatic ester properties with worse results for PA whose structure is not fully captured by the simulations. The fluid structure is characterized by domains formed by aromatic rings and ester groups with apolar regions formed by alkylic chains with increasing importance as these chain lengths increase.

The results reported in this work show that a combined experimental/theoretical approach to study fluid properties and structure is a very valuable tool because it provides deep molecular level insights that may be connected with the accurate macroscopic thermophyisical data. Hence, the combination of thermodynamics with molecular modeling for industrially relevant solvents may provide valuable information required for practical and/or theoretical purposes that circumvent the well-known problems to develop structure−property relationships and that allows us to obtain reliable predictions of required properties in pressure/temperature conditions for which it is difficult to do measurements. This approach will be extended in future works for other selected pure and/or mixed fluids.

Acknowledgment. The financial support by Junta de Castilla y León, Project BU10/03, and Ministerio de Educación y Ciencia, Spain, Project CTQ2005-06611/PPQ, is gratefully acknowledged.

Supporting Information Available: Densities, TRIDEN fitting coefficients of densities, isobaric expansibilities, isothermal compressibilities, internal pressures, EOS parameters, and parameters for IEF-PCM calculations. This material is available free of charge via the Internet at http://pubs.acs.org.

References and Notes

(1) Archer, W. L. *Industrial Solvents Handbook*; Marcel Dekker: New York, 1996.

(2) Marcus, Y. *The Properties of Solvents*; Wiley: New York, 1998.

(3) Buncel, E.; Stairs, R. A.; Wilson, H. *The Role of Solvents in Chemical Reactions*; Oxford University Press: New York, 2003.

(4) Reichardt, C. *Solvents and Solvent Effects in Organic Chemistry*, 3rd ed.; Wiley-VCH: Weinheim, Germany, 2003.

(5) Seider, W. D.; Seader, J. D.; Lewin, D. R. *Product and Process Design Principles: Synthesis, Analysis, and Evaluation*, 2nd ed.; Wiley: New York, 2003.

(6) Chen, C. C.; Mathias, P. M. *AIChE J.* **2002**, *48*, 194.

(7) Dohrn, R.; Pfohl, O. *Fluid Phase Equilib.* **2002**, *15*, 194−197.

(8) Raal, J. D.; Muhlbauer, A. L. *Phase Equilibria: Measurement and Computation*; Taylor and Francis: Washington, DC, 1998.

(9) Prausnitz, J. M.; Lichtenthaler, R. M.; Gomes de Azevedo, E. *Molecular Thermodynamics of Fluid Phase Equilibria*, 3rd ed.; Prentice-Hall: Upper Saddle River, NJ, 1999.

(10) (a) Tsierkezos, N. G.; Kelarakis, A. E.; Molinou, I. E. *J. Chem. Eng. Data* **2000**, *45*, 776. (b) Semeniuk, B.; Wilczura-Wachnick, H. *Fluid Phase Equilib.* **1998**, *152*, 337. (c) Ortega, J.; Postigo, M. A. *Fluid Phase Equilib.* **1995**, *108*, 121. (d) García, B.; Ortega, J. C. *J. Chem. Eng. Data* **1988**, *33*, 200. (e) García, B.; Ortega, J. C. *Thermochim. Acta* **1987**, *117*, 219. (f) Aminabhavi, T. M.; Raikar, S. K. *Collect. Czech. Commun.* **1993**, *58*, 1761. (g) Aminabhavi, T. M.; Phayde, H. T. S.; Khinnavar, R. S.; Gopalakrishna, B. *J. Chem. Eng. Data* **1994**, *39*, 251. (h) Dusart, O.; Piekarski, C.; Piekarski, S.; Viallard, A. *J. Chim. Phys.* **1976**, *78*, 837. (i) Grolier, J. P. E.; Ballet, D.; Viallard, A. *J. Chem. Thermodyn.* **1974**, *6*, 895.

(11) (a) García, B.; Alcalde, R.; Aparicio, S.; Leal, J. M. *Ind. Eng. Chem. Res.* **2002**, *41*, 4399. (b) García, B.; Alcalde, R.; Aparicio, S.; Leal, J. M. *Phys. Chem. Chem. Phys.* **2002**, *4*, 5833. (c) García, B.; Aparicio, S.; Alcalde, R.; Leal, J. M. *J. Phys. Chem. B* **2003**, *107*, 13478. (d) García, B.; Aparicio, S.; Navarro, A. M.; Alcalde, R.; Leal, J. M. *J. Phys. Chem. B* **2004**, *108*, 15841. (e) Aparicio, S.; Alcalde, R.; Leal, J. M.; García, B. *J. Phys. Chem. B* **2005**, *109*, 6375. (f) Aparicio, S.; Alcalde, R.; García, B.; Leal, J. M. *Ind. Eng. Chem. Res.* **2005**, *44*, 7575. (g) Alcalde, R.; Aparicio, S.; García, B.; Leal, J. M. *J. Phys. Chem. B* **2005**, *109*, 19908.

(12) *Equations of State for Fluids and Fluid Mixtures*; Sengers, J. V., Kayser, R. F., Peters, C. J., White, H. J., Eds.; Elsevier: Amsterdam, 2000.

(13) Valderrama, J. O. *Ind. Eng. Chem. Res.* **2003**, *42*, 1603.

(14) Wertheim, M. S. *J. Chem. Phys.* **1986**, *85*, 2929.

(15) (a) Chapman, W. G.; Gubbins, K. E.; Jackson, G.; Radosz, M. *Ind. Eng. Chem. Res.* **1990**, *29*, 1709. (b) Huang, S. H.; Radosz, M. *Ind. Eng. Chem. Res.* **1990**, *29*, 2284.

(16) Gross, J.; Sadowski, G. *Ind. Eng. Chem. Res.* **2001**, *40*, 1244.

(17) (a) García, B.; Aparicio, S.; Alcalde, R.; Dávila, M. J.; Leal, J. M. *Ind. Eng. Chem. Res.* **2004**, *43*, 3205. (b) Aparicio, S.; García, B.; Alcalde, R.; Dávila, M. J.; Leal, J. M. *J. Phys. Chem. B* **2006**, *110*, 6933.

(18) Lemmon, E. W.; McLinden, M. O.; Friend, D. G. Thermophysical Properties of Fluid Systems. In *NIST Chemistry WebBook*; Linstrom, P. J., Mallard, W. G., Eds.; NIST Standard Reference Database Number 69; National Institute of Standards and Technology: Gaithersburg, MD, 2003. http://webbook.nist.gov.

(19) (a) Fandiño, O.; Pensado, A. S.; Lugo, L.; López, E. R.; Fernández, J. *Green Chem.* **2005**, *7*, 775. (b) Lundstrum, R.; Goodwin, A. R. H.; Hsu, K.; Frels, M. F.; Caudwell, D. R.; Trusler, J. P. M. *J. Chem. Eng. Data* **2005**, *50*, 1377. (c) Bernhardt, J.; Pauly, H. *J. Phys. Chem.* **1980**, *84*, 145. (d) Ashcroft, S. J.; Booker, D. R.; Turner, J. C. R. *J. Chem. Soc., Faraday Trans.* **1990**, *86*, 145.

(20) Frisch, M. J.; Trucks, G. W.; Schlegel, H. B.; Scuseria, G. E.; Robb, M. A.; Cheeseman, J. R.; Montgomery, J. A., Jr.; Vreven, T.; Kudin, K. N.; Burant, J. C.; Millam, J. M.; Iyengar, S. S.; Tomasi, J.; Barone, V.; Mennucci, B.; Cossi, M.; Scalmani, G.; Rega, N.; Petersson, G. A.; Nakatsuji, H.; Hada, M.; Ehara, M.; Toyota, K.; Fukuda, R.; Hasegawa, J.; Ishida, M.; Nakajima, T.; Honda, Y.; Kitao, O.; Nakai, H.; Klene, M.; Li, X.; Knox, J. E.; Hratchian, H. P.; Cross, J. B.; Bakken, V.; Adamo, C.; Jaramillo, J.; Gomperts, R.; Stratmann, R. E.; Yazyev, O.; Austin, A. J.; Cammi, R.; Pomelli, C.; Ochterski, J. W.; Ayala, P. Y.; Morokuma, K.; Voth, G. A.; Salvador, P.; Dannenberg, J. J.; Zakrzewski, V. G.; Dapprich, S.; Daniels, A. D.; Strain, M. C.; Farkas, O.; Malick, D. K.; Rabuck, A. D.; Raghavachari, K.; Foresman, J. B.; Ortiz, J. V.; Cui, Q.; Baboul, A. G.; Clifford, S.; Cioslowski, J.; Stefanov, B. B.; Liu, G.; Liashenko, A.; Piskorz, P.; Komaromi, I.; Martin, R. L.; Fox, D. J.; Keith, T.; Al-Laham, M. A.; Peng, C. Y.; Nanayakkara, A.; Challacombe, M.; Gill, P. M. W.; Johnson, B.; Chen, W.; Wong, M. W.; Gonzalez, C.; Pople, J. A. *Gaussian 03*, revision C.02; Gaussian, Inc.: Wallingford, CT, 2004.

(21) Becke, A. D. *Phys. Rev. A* **1988**, *38*, 3098.

(22) Lee, C.; Yang, W.; Parr. R. G. *Phys. Rev. B* **1988**, *37*, 785.

(23) Becke, A. D. *J. Chem. Phys.* **1993**, *98*, 5648.

(24) Singh, U. C.; Kollman, P. A. *J. Comput. Chem.* **1984**, *5*, 129.

(25) Besler, B. H.; Merz, K. M.; Kollman, P. A. *J. Comput. Chem.* **1990**, *11*, 431.

(26) (a) Ponder, J. W. *TINKER: Software Tool for Molecular Design*, version 4.2; Washington University School of Medicine: St. Louis, MO, 2004. (b) Storz, C. *J. Comput. Chem.* **2005**, *26*, 471. (c) Lei, Y.; Li, H.; Zhang, R.; Han, S. *J. Phys. Chem. B* **2004**, *108*, 10131. (d) Grossman, J. C.; Schewegler, E.; Galli, G. *J. Phys. Chem. B* **2004**, *108*, 15865. (e) Lei, Y.; Li, H.; Pan, H.; Han, S. *J. Phys. Chem. B* **2003**, *107*, 1574.

(27) Hoover, W. G. *Phys. Rev. A* **1985**, *31*, 1695.

(28) Allen, M. P.; Tildesley, D. J. *Computer Simulation of Liquids*; Clarendon Press: Oxford, U. K., 1989.

(29) Rickaert, J. P.; Ciccotti, G.; Berendsen, H. J. *J. Comput. Phys.* **1977**, *23*, 327.

(30) Essmann, U. L.; Perera, M. L.; Berkowitz, T.; Darden, H.; Lee, H.; Pedersen, L. G. *J. Chem. Phys.* **1995**, *103*, 8577.

(31) (a) Martínez, J. M.; Martínez, L. *J. Comput. Chem.* **2003**, *24*, 819. (b) Friedlander, A.; Martínez, J. M.; Santos, S. A. *Appl. Math. Opt.* **1994**, *30*, 235.

(32) Jorgensen, W. L.; Maxwell, D. S.; Tirado−Rives, J. *J. Am. Chem. Soc.* **1996**, *118*, 11225.

(33) (a) Rizzo, R. C.; Jorgensen, W. L. *J. Am. Chem. Soc.* **1999**, *121*, 4827. (b) McDonald, N. A.; Jorgensen, W. L. *J. Phys. Chem. B* **1998**, *102*, 8049. (c) Kaminski, G.; Duffy, E. M.; Matsui, T.; Jorgensen, W. L. *J. Phys. Chem.* **1994**, *98*, 13077.

(34) Ihmehls, E. C.; Gmehling, J. *Ind. Eng. Chem. Res.* **2001**, *40*, 4470.

(35) (a) Cibulka, I. *Fluid Phase Equilib.* **1993**, *89*, 1. (b) Gomes de Azevedo, R.; Esperanca, J. M. M. S.; Najdanovic−Visak, V.; Visak, Z. P.; Guedes, H. J. R.; Nunes da Ponte, M.; Rebelo, L. P. N. *J. Chem. Eng. Data* **2005**, *50*, 997. (c) Gu, Z.; Brennecke, J. F. *J. Chem. Eng. Data* **2002**, *47*, 339. (d) Morrow, T. I.; Maginn, E. J. *J. Phys. Chem. B* **2002**, *106*, 12807. (d) Rebelo, L. P. N.; Najdanovic-Visak, V.; Visak, Z. P.; Nunes da Ponte, M.; Szydlowski, J.; Cerdeiriña, C. A.; Troncoso, J.; Romaní, L.; Esperanca, J. M. S. S.; Guedes, H. J. R.; de Sousa, H. C. *Green Chem.* **2004**, *6*, 369.

(36) Dack, M. R. J. *Chem. Soc. Rev.* **1975**, *4*, 211.

(37) Hansen, C. M. *Hansen Solubility Parameters: A User's Handbook*; CRC Press: Boca Raton, FL, 2000.

(38) Steele, W. V.; Chirico, R. D.; Cowell, A. B.; Knipmeyer, S. E.; Nguyen, A. *J. Chem. Eng. Data* **2002**, *47*, 667.

(39) Korea Thermophysical Properties Data Bank. http://www.cheric.org/kdb/.

(40) Wilson, G. M.; VonNiederhausern, D. M.; Giles, N. F. *J. Chem. Eng. Data* **2002**, *47*, 761.

(41) Poling, B. E.; Prausnitz, J. M.; O'Connell, J. P. *The Properties of Gases and Liquids*, 5th ed.; McGraw-Hill: New York, 2000.

(42) (a) Pfohl, O.; Pagel, A.; Brunner, G. *Fluid Phase Equilib.* **1999**, *157*, 53. (b) Gupta, R. B.; Johnston, K. P. *Fluid Phase Equilib.* **1994**, *99*, 135. (c) Pfohl, O.; Budich, M. *Fluid Phase Equilib.* **2001**, *189*, 179. (d) Wolbach, J.; Sandler, S. I. *Ind. Eng. Chem. Res.* **1998**, *37*, 2917.

(43) (a) Luck, W. A. P. *Angew. Chem., Int. Ed. Engl.* **1980**, *19*, 28. (b) Ludwig, R. *Phys. Chem. Chem. Phys.* **2002**, *4*, 5481.

(44) Karakatsani, E. K.; Spyriouni, T.; Economou, I. G. *AIChE J.* **2005**, *51*, 2328.

(45) Nelson, M. R.; Borkman, R. F. *J. Mol. Struct. (THEOCHEM)* **1998**, *432*, 247.

(46) Hummel, J. P.; Flory, P. J. *Macromolecules* **1980**, *13*, 479.

(47) Januszko, A.; Kaszynski, P.; Drzewinski, W. *J. Mater. Chem.* **2006**, *16*, 452.

(48) Abraham, R. J.; Bardsley, B.; Mobli, M.; Smith, R. J. *Magn. Reson. Chem.* **2005**, *43*, 3.

(49) Imase, T.; Kawauchi, S.; Watanabe, J. *Macromol. Theor. Simul.* **2001**, *10*, 434.

(50) Shibakami, M.; Sekiya, A. *Acta Crystallogr., Sect. C: Cryst. Struct. Commun.* **1995**, *51*, 326.

(51) Maheswari, S.; Chowdhury, A.; Sathyamurthy, S.; Mishra, H.; Tripathi, H. B.; Panda, M.; Chandrasekhar, J. *J. Phys. Chem. A* **1999**, *103*, 6257.

(52) Anandan, K.; Kolandaivel, P.; Kumaresan, R. *Int. J. Quantum Chem.* **2005**, *103*, 127.

(53) Palomar, J.; De Paz, J. L. G.; Catalán, J. *Chem. Phys.* **1999**, *246*, 167.

(54) Simon, S.; Duran, M.; Dannenberg, J. J. J. *Chem. Phys.* **1996**, *105*, 11024.

(55) Cances, E.; Mennucci, B. *J. Math. Chem.* **1998**, *23*, 309.

(56) Weast, R. C.; Graselli, J. G. *CRC Handbook of Organic Compounds*; CRC Press: Boca Raton, FL, 1989.

(57) Majer, V.; Svoboda, V. *Enthalpies of Vaporization of Organic Compounds*; Blackwell Scientific: Oxford, U. K., 1985.

(58) Aminabhavi, T. M.; Phayde, H. T. S.; Khinnavar, R. S. *Collect. Czech. Commun.* **1994**, *59*, 1511.